Microscopic processes in dielectrics under irradiation by subpicosecond laser pulses

A. Kaiser*
Institut für Theoretische Physik der Technischen Universität Braunschweig, Mendelssohnstraße 3, D-38106 Braunschweig, Germany and Max-Planck-Institut für Physik komplexer Systeme, Nöthnitzer Straße 38, D-01187 Dresden, Germany

B. Rethfeld†
Institut für Theoretische Physik der Technischen Universität Braunschweig, Mendelssohnstraße 3, D-38106 Braunschweig, Germany and Institut für Laser- und Plasmaphysik der Universität Essen, D-45117 Essen, Germany

M. Vicanek and G. Simon
Institut für Theoretische Physik der Technischen Universität Braunschweig, Mendelssohnstraße 3, D-38106 Braunschweig, Germany
(Received 4 August 1999; revised manuscript received 29 November 1999)

Transparent solids may show strong absorption when irradiated by a high-intensity laser pulse. Such laser induced breakdown is due to the formation of a free-electron gas. We investigate theoretically the role of ionization processes in a defect-free crystal, including in our model two competing processes: strong-electric-field ionization and electron impact ionization. Free-electron heating is described in terms of electron-phonon-photon collisions. Relaxation of the free electron gas occurs through electron-electron collisions and electron-phonon collisions. The latter are also responsible for energy transfer from the free-electron gas to the phonon gas. We solve numerically a system of time dependent Boltzmann equations, where each considered process is included by its corresponding collision integral. Our results show formation, excitation, and relaxation of the electron gas in the conduction band. We find that strong-electric-field ionization is mainly responsible for free-electron generation. No avalanche occurs at femtosecond laser irradiation. The electron density and the internal energies of the subsystems are calculated. Critical fluences obtained using various criteria for damage threshold are in good agreement with recent experiments.

I. INTRODUCTION

Interaction of solids with ultrashort laser pulses involves a number of microscopic processes. When transparent solids are irradiated with laser intensities above a certain threshold, strong absorption of the laser energy occurs, known as laser-induced breakdown.[1–10] The microscopic processes which cause this change of an initially transparent material to an absorbing solid with metallic behavior act on femtosecond time scales. Laser pulses with a duration of only a few tens of femtoseconds provide new possibilities to investigate these processes.[4–9]

The mechanisms which lead to breakdown in dielectrics can be divided into extrinsic and intrinsic mechanisms.[2,3,10] Extrinsic breakdown is caused by defects and impurities in the material, where local absorption is much higher than it would be in a pure material. Intrinsic breakdown is a process which is characteristic of the material itself as a monocrystal dielectric without defects. In our work we consider only intrinsic processes, thereby clarifying the role of breakdown mechanisms like multiphoton ionization and electron avalanche. Ionization processes may lead to a rather high free-electron density, which fact can explain the metal-like behavior of dielectrics under ultrashort laser pulse irradiation found by many authors.[1–7,11] The processes responsible for the formation of a free-electron gas are illustrated in Fig. 1.

Multiphoton ionization is an effect of a strong electric field. In very high electric laser fields, also tunnel ionization may occur.[2–4,12,13] Both processes shift electrons from the valence band to the conduction band with help of the electric laser field, hence we call them strong-electric-field ionization. In contrast, impact ionization may be effected by an existing free electron in the conduction band. If its kinetic energy is sufficiently large, it may transfer part of it to an electron in the valence band, thus enable it to overcome the ionization potential.[1–4,7,14–19]

The effect of all ionization processes results in the formation of a free electron gas, leading to metallic behavior of even a wide-band-gap material. The strong-electric-field ionization and impact ionization, which may lead to an avalanche, are two competing processes. Several theoretical and experimental investigations have already been carried out to clarify the role of these processes.[2–4,7,15,16] A common as-

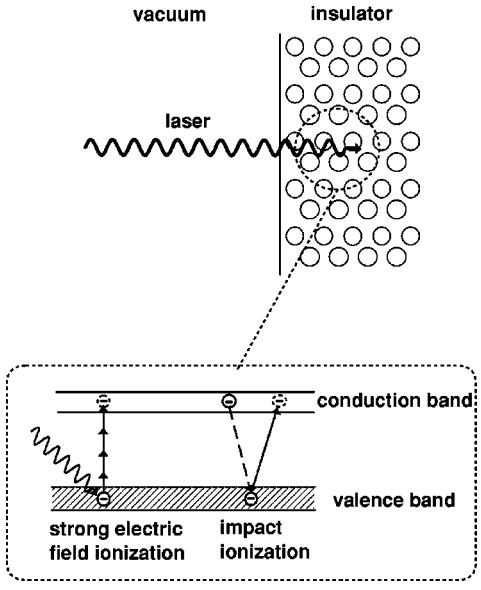

FIG. 1. Processes for generation of free electron gas.

sumption is that strong-electric-field ionization leads to a few starting electrons whereas an avalanche produced by impact ionization is responsible for the breakdown.[1–4,14,16] However, for subpicosecond lasers it is proposed that strong-electric-field ionization becomes more important than impact ionization, although the latter may constitute a significant quantitative modification.[2,3,7,15,16]

In the following Sec. II we present our theoretical model and its application to dielectrics. The collision processes and the corresponding matrix elements are described in Sec. III. Results for SiO_2 are presented in Sec. V. We show the distribution function of the laser-induced free electron gas and phonon gas and their perturbations due to laser irradiation. The roles of strong-electric-field ionization and impact ionization are investigated. Furthermore, we calculate the energy density stored in the free electron gas and phonon gas, as well as the total absorbed energy amount in the crystal. Using various criteria for crystal damage, we calculate threshold fluences which are in good agreement with recent experiments.

II. MAIN ASSUMPTIONS

A. Microscopical processes in dielectrics

To investigate the correlation and interplay of collision processes in dielectrics irradiated with subpicosecond laser pulses, we choose a transport theoretical approach because the initial thermal equilibrium of the electron and phonon gas is strongly perturbed through interaction with the laser pulse. We use Boltzmann's equation to describe the interaction of electrons and phonons with the laser beam and among each other, taking microscopic collision processes into account. In contrast to averaged phenomenological descriptions, our model accounts for the dependence of the collision probability on each particular particle's energy. Each considered collision process is included as a collisional term in the Boltzmann equation. For the absorption of a laser pulse by a dielectric material, a free electron gas has to be created first. We consider the formation of free electrons in the kinetic description, including strong-electric-field ionization[3,7,12,13,15,16] and impact ionization, which may lead to an avalanche,[3,7,14–17,20–24] by appropriate collision integrals. The free-electron kinetic energy of the electron gas in the conduction band increases by absorbing photons in electron-phonon-photon collisions.[18,25] These collisions lead to a high excitation of the free electron gas, far from thermal equilibrium. Electron-electron collisions and electron-phonon collisions, in turn, work towards thermal equilibrium within the electron gas at higher temperature. Furthermore, energy is transferred to the phonon gas by electron-phonon collisions, resulting in a diminished free-electron kinetic energy.

Recently, Stuart *et al.*[7,8,26] investigated the breakdown in dielectrics by short-pulse laser irradiation in a kinetic approach using a Fokker-Planck equation. There are further works in which diffusion equations were used.[15,18,19] In our approach, we focus the investigation on the femtosecond regime, therefore we consider all collision processes microscopically using matrix elements for transition probability which are derived by quantum-mechanical first order pertubation theory. We prefer to use complete collision integrals of Boltzmann equation rather than a diffusion equation to avoid any phenomenological parameter in our calculation. We consider this approach as necessary, since we expect that the free-electron distribution function does neither keep its shape nor is stationary but instead shows a highly non-linear, dynamical behavior.

In our model, we consider three phonon modes, each of them is described by a Boltzmann equation. The coupling between free-electron gas and phonon gas and the laser absorption by free electrons is treated in terms of appropriate collision integrals, thus obtaining a system of coupled Boltzmann equations. A spatially uniform electric laser field is assumed, which is justified in dielectrics with a large penetration depth. We assume irradiation of a perfect crystal without lattice deformation or ablation during the pulse.

B. Crystal

We assume a perfect homogeneous and isotropic crystal without defects. No defects should be created during and after the laser pulse. Actually, defect creation by electron recombination after short times has been reported,[2,3,9] however the microscopical description of this process is still only rudimentarily developed. Since we focus on short time excitation dynamics, we do not consider any recombination process here.

The laser beam should penetrate nearly homogeneously into the crystal. Therefore we neglect spatial dependence of the problem and, in particular, we do not consider transport.

With these assumptions, the occupation numbers f of electrons and g of phonons depend only on time and momentum.

C. Electrons

We assume parabolic energy dispersion of electrons in the conduction and in valence band. The effective masses in the conduction band $m^\star$ and in the valence band $m_v^\star$, respectively, are both assumed to be equal to the free electron mass.

The Fermi level is supposed to be located at the center of the bandgap Δ which, for α-quartz (α-SiO_2), is assumed to be $\Delta = 9$ eV.[7,20,21] Because free electrons oscillate in the electric laser field, the corresponding oscillation energy has to be provided in addition to the bandgap when an electron is to be shifted from the valence band into the conduction band. Thus we assume an effective ionization potential $\tilde{\Delta}$ which reads[12]

$$\tilde{\Delta} = \Delta + \frac{e^2 E_L^2}{4 m_{\mathrm{redu}} \Omega^2}, \tag{1}$$

where Δ is the bandgap, Ω and E_L the frequency and amplitude of electric laser field, respectively, and $1/m_{\mathrm{redu}} = 1/m^\star + 1/m_v^\star$ is the reduced effective mass. The second term in the sum accounts for the oscillation energy of the electron due to the electric laser field.

D. Phonons

In our model electrons interact only with longitudinal phonons (see below). As we do not consider heat conduction,

we expect phonon-phonon collisions to be unimportant at ultrashort time scales. Therefore, we can neglect transversal phonon modes.

Acoustical phonons are described by Debye's model with sound velocity $v_s = 5935$ m/s for SiO_2 and Debye's wave vector $q_{\mathrm{Debye}} = 2.35 \times 10^{10}$ m^{-1}.[16,27,28] Optical phonons are described by Einstein's model assuming the edge of Brillouin's zone coincident with Debye's wave vector.[27] In SiO_2 there are two optical modes; for the first we assume an energy of 63 meV and for the second an energy of 153 meV.[16,20,29] If the model is applied for ionic crystals, also polar modes have to be taken into account.[20,22] We consider only normal processes—umklapp processes are neglected.

III. MATHEMATICAL DESCRIPTION

Since we neglect spatial dependence of wave vectors and polarization and consider no spatial transport in our model, the system of Boltzmann equations depends only on time and energy of electrons and phonons. Therefore, the left hand side of the Boltzmann equations for the occupation numbers contains only a time derivative.

We calculate the time evolution of the occupation number of free electrons in the conduction band and of the occupation number of each phonon mode. For electrons in the valence band we assume a constant occupation number, which means that the valence band is always completely filled. Furthermore we neglect electron spin-spin interaction, therefore we need only one equation for the electron occupation number.

The collision term for the electron occupation number f consists of individual expressions for each considered process. In our model we include electron-electron (e-e) and electron-phonon (e-ph) interactions, phonon-assisted photon absorption (e-ph-pt), strong-electric-field ionization (sefi) and electron impact ionization (imp).

For phonons, we consider several modes of acoustical and optical phonons using one Boltzmann equation for occupation number g_β of each mode β. Because phonon-phonon interaction is neglected, the Boltzmann equation for phonons contains only collision terms of phonon-electron interaction and phonon-electron-photon interaction. Although phonons do not directly absorb energy from the laser, they are indirectly affected by irradiation due to their interaction with photon-absorbing electrons.

The Boltzmann equations represent a system of coupled, nonlinear, time dependent integro-differential equations which read

$$\left(\frac{\partial}{\partial t}\right) f(\boldsymbol{k},t) = \left(\frac{\partial f(\boldsymbol{k},t)}{\partial t}\right)_{\text{e-e}} + \left(\frac{\partial f(\boldsymbol{k},t)}{\partial t}\right)_{\text{e-ph}} + \left(\frac{\partial f(\boldsymbol{k},t)}{\partial t}\right)_{\text{e-ph-pt}} + \left(\frac{\partial f(\boldsymbol{k},t)}{\partial t}\right)_{\text{imp}} + \left(\frac{\partial f(\boldsymbol{k},t)}{\partial t}\right)_{\text{sefi}}, \tag{2}$$

$$\left(\frac{\partial}{\partial t}\right) g_\beta(\boldsymbol{q},t) = \left(\frac{\partial g_\beta(\boldsymbol{q},t)}{\partial t}\right)_{\text{ph-e}} + \left(\frac{\partial g_\beta(\boldsymbol{q},t)}{\partial t}\right)_{\text{ph-e-pt}}. \tag{3}$$

Before irradiation, electrons are assumed to obey a Fermi-Dirac distribution, while phonons obey a Bose-Einstein distribution, both at room temperature. In the following we describe the approach for each considered process separately.

A. Electron-electron collisions

Electron-electron interaction is a relaxation process which works towards thermal equilibrium within the free-electron gas.

The interaction is described by a screened Coulomb potential which results in a matrix element[22–24]

$$|\mathcal{M}_{\text{e-e}}(\boldsymbol{k},\boldsymbol{k}_2;\boldsymbol{k}_1,\boldsymbol{k}_3)|^2 := |\langle c\boldsymbol{k}, c\boldsymbol{k}_2 | V_{\text{e-e}} | c\boldsymbol{k}_1, c\boldsymbol{k}_3\rangle|^2 = \left(\frac{e^2}{\varepsilon_0 V}\frac{1}{(\boldsymbol{k}_2-\boldsymbol{k}_3)^2+q_0^2}\right)^2 \delta_{\boldsymbol{k}+\boldsymbol{k}_2,\boldsymbol{k}_1+\boldsymbol{k}_3}. \tag{4}$$

Here $\boldsymbol{k}$ and $\boldsymbol{k}_2$ are the wave vectors of two electrons before collision, and $\boldsymbol{k}_2-\boldsymbol{k}_3=\boldsymbol{k}_1-\boldsymbol{k}$ is their exchanged momentum. We assume the inverse screening length q_0 equal to Debye's screening length, given by

$$q_0^2 = \frac{e^2 n}{\varepsilon_0 k_B T_e}, \tag{5}$$

where n is the free electron density and T_e is the temperature of the electron gas. The free electron density can be determined self-consistently during our calculation. For the temperature T_e we choose a constant value of 5000 K. Since the electron gas is strongly disturbed and not in equilibrium, the concept of temperature is not strictly valid. However, for the calculation of the screening length this is of minor importance, because the variation of electron density affects the screening dynamics much stronger. Here we want to point out that T_e is the only nonmaterial parameter in our model, but this can be avoided if the expression from Binder *et al.*[30] is used for q_0.

Because we assume a crystal which is homogeneous in space and isotropic with respect to momentum, the collision integral[22–24,31,32] may be reduced from six dimensions to two[32,33] which reads, in terms of energy variables

$$\left(\frac{\partial f(\varepsilon)}{\partial t}\right)_{\text{e-e}} = \frac{1}{\hbar^4}\left(\frac{m^\star}{2\pi\hbar}\right)^3\left(\frac{e^2}{\varepsilon_0}\right)^2\frac{1}{k}\int_{\{\varepsilon_1+\varepsilon_3\geqslant\varepsilon\}} d\varepsilon_1 d\varepsilon_3 \times [f(\varepsilon_1)f(\varepsilon_3)(1-f(\varepsilon))(1-f(\varepsilon_2)) - f(\varepsilon)f(\varepsilon_2)(1-f(\varepsilon_1))(1-f(\varepsilon_3))] \times \int_{\mathcal{K}} \frac{d\kappa}{(\kappa^2+q_0^2)^2}, \tag{6}$$

with $\varepsilon_2=\varepsilon_1+\varepsilon_3-\varepsilon$, where ε_i is the kinetic energy of an electron with wave number $k_i := k(\varepsilon_i) = \sqrt{2m^\star\varepsilon_i/\hbar^2}$. The last integral over the integration region $\mathcal{K}$ can be solved analytically. $\mathcal{K}$ is given by

$$\mathcal{K} = [|k-k_3|, k+k_3) \cap (|k_1-k_2|, k_1+k_2],$$

and follows from conservation of energy and momentum.

B. Electron impact ionization

Impact ionization takes place by free electrons of high kinetic energy, which may transfer sufficient energy to valence electrons to overcome the ionization potential. Impact ionization leads to an increased electron density in the conduction band.

For this process a minimum kinetic energy of the colliding free electron is needed to fulfill energy *and* momentum conservation. This critical energy reads[17,23,32]

$$\varepsilon_c = \frac{1+2\mu}{1+\mu}\tilde{\Delta} \quad \text{with} \quad \mu = \frac{m^\star}{m_v^\star}. \tag{7}$$

In the case of $m^\star$ and $m_v^\star$ being both equal to the free electron mass, the critical energy is higher than the ionization potential by a factor of 1.5. Including momentum conservation, our model leads to a higher critical energy and therefore a lower probability for impact ionization compared to other approaches.[7,16]

A common treatment for impact ionization is the application of the so-called Keldysh's impact ionization formula

$$W_{\text{imp}}(\varepsilon) = P \cdot ((\varepsilon - \varepsilon_c)/\varepsilon_c)^2, \tag{8}$$

where P is constant. This expression gives the impact ionization for a free electron with kinetic energy ε above the critical energy ε_c shifting an electron from valence band into conduction band.[16,17,23,26] In the derivation of Eq. (8) it was assumed that the excess kinetic energy $\varepsilon - \varepsilon_c$ is small ($\ll \varepsilon_c$).[17] When applying Eq. (8) it is usually assumed that the excess kinetic energy is equally divided between the two resulting electrons.[16,26] Our calculations show, however, that the resulting electrons can have different energies. This can become important at high free electron densities when Pauli's principle influences the probability of the process.

Therefore we avoid applying the approximation (8), moreover, in our calculations we consider electrons at much higher energies $\varepsilon - \varepsilon_c \approx \varepsilon_c$. Thus we implement the impact ionization process in term of a corresponding collision integral. The matrix element for impact ionization is given by the product of the matrix element for screened electron-electron interaction and the probability for a band transition:[22–24]

$$\begin{aligned} |\mathcal{M}_{\text{imp}}(\boldsymbol{k},\boldsymbol{k}_2;\boldsymbol{k}_1,\boldsymbol{k}_3)|^2 &:= |\langle c\boldsymbol{k}, c\boldsymbol{k}_2 | V_{\text{e-e}} | c\boldsymbol{k}_1, v\boldsymbol{k}_3 \rangle|^2 \\ &= |\mathcal{M}_{\text{e-e}}(\boldsymbol{k},\boldsymbol{k}_2;\boldsymbol{k}_1,\boldsymbol{k}_3)|^2 \cdot |I(\boldsymbol{k}_2,\boldsymbol{k}_3)|^2, \end{aligned} \tag{9}$$

where $|I(\boldsymbol{k}_2,\boldsymbol{k}_3)|$ is the overlap integral which follows from $\boldsymbol{p}\cdot\boldsymbol{k}$ theory and f-sum rule,[23]

$$|I(\boldsymbol{k}_2,\boldsymbol{k}_3)|^2 = \frac{\hbar^2}{2\tilde{\Delta}}\left(\frac{1}{m} + \frac{1}{m_v^\star}\right)|\boldsymbol{k}_2 - \boldsymbol{k}_3|^2. \tag{10}$$

Here, m is the free electron mass.

Using this matrix element, it is possible[23] to calculate the constant P of Keldysh's impact ionization formula (8) for $\varepsilon \approx \varepsilon_c$ resulting to $P = 21.2\ \text{fs}^{-1}$ for our material parameters. This value is more than one magnitude larger than the value of $1.5\ \text{fs}^{-1}$ chosen by other authors.[16,26] Thus, compared with the results of Refs. 16 and 26, it has to be expected that our collision integral yields much stronger impact ionization.

With the same assumption as for the electron-electron collisions, the collision integral of the impact ionization may be reduced from six to two dimensions and reads, in terms of energy variables[32]

$$\begin{aligned} \left(\frac{\partial f(\varepsilon)}{\partial t}\right)_{\text{imp}} = {} & \frac{1}{(2\pi\hbar)^3}\left(\frac{e^2}{\varepsilon_0}\right)^2 \frac{\hbar^2}{2\tilde{\Delta}}\left(\frac{m_v^\star}{m}+1\right)\left(\frac{m^\star}{\hbar^2}\right)^2 \frac{1}{k}\Bigg\{ \int_{\{\varepsilon_1-\varepsilon-\varepsilon_2 \geqslant \tilde{\Delta}\}} d\varepsilon_1 d\varepsilon_2 [f(\varepsilon_1) f_v(\varepsilon_3^a)(1-f(\varepsilon))(1-f(\varepsilon_2))] \\ & \times \left(\int_{\mathcal{K}_a} d\kappa \frac{\kappa^2}{(\kappa^2+q_0^2)^2} + \int_{\mathcal{K}_b} d\kappa \frac{\kappa^2}{(\kappa^2+q_0^2)^2} \right) - \int_{\{\varepsilon-\varepsilon_1-\varepsilon_2 \geqslant \tilde{\Delta}\}} d\varepsilon_1 d\varepsilon_2 [f(\varepsilon) f_v(\varepsilon_3^c)(1-f(\varepsilon_1))(1-f(\varepsilon_2))] \\ & \times \int_{\mathcal{K}_c} d\kappa \frac{\kappa^2}{(\kappa^2+q_0^2)^2} \Bigg\}, \end{aligned} \tag{11}$$

where the kinetic electron energies $\varepsilon_3^a = m_v^\star/m^\star(\varepsilon_1 - \varepsilon - \varepsilon_2 - \tilde{\Delta})$ and $\varepsilon_3^c = m_v^\star/m^\star(\varepsilon - \varepsilon_1 - \varepsilon_2 - \tilde{\Delta})$ follow from energy conservation. The electron wave numbers are given by $k_i := k(\varepsilon_i) = \sqrt{2m^\star\varepsilon_i/\hbar^2}$. Again, the integrals over the regions $\mathcal{K}_a, \mathcal{K}_b, \mathcal{K}_c$ can be solved analytically, where $\mathcal{K}_a, \mathcal{K}_b, \mathcal{K}_c$ are boundary conditions which result from energy and momentum conservation and read

$$\mathcal{K}_a := [|k_1 - k|, k_1 + k) \cap (|k_2 - k_3^a|, k_2 + k_3^a],$$

$$\mathcal{K}_b := [|k_3^a - k|, k_3^a + k) \cap (|k_1 - k_2|, k_1 + k_2],$$

$$\mathcal{K}_c := [|k_1 - k|, k_1 + k) \cap (|k_2 - k_3^c|, k_2 + k_3^c].$$

C. Strong-electric-field ionization

In strong electric laser fields, an electron in the valence band may absorb several photons in one step and so gain enough energy to overcome the ionization potential.[2,3,12,13] This process is called multiphoton ionization; its probability, of course, increases with laser intensity. For very high electric laser fields, the potential well formed by the band gap is distorted and photo-induced tunneling may occur.

Keldysh examined strong-electric-field ionization,[12] and obtained a general expression for the ionization rate and approximate expressions for both limiting cases. A criterion to decide between either of the processes is given by the pa-

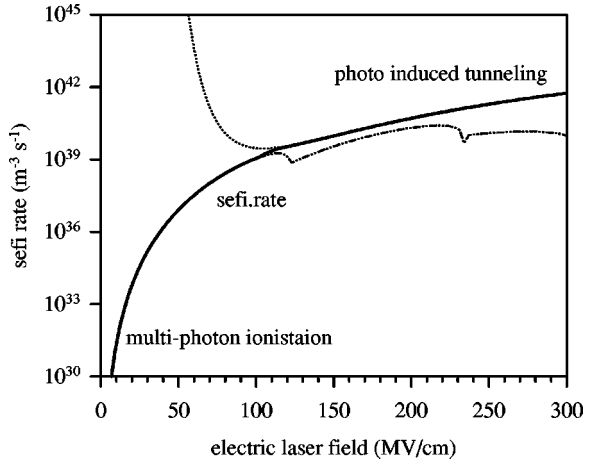

FIG. 2. Rates for strong-electric-field ionization (sefi) according to Keldysh (1965). Parameters for 500 nm laser beam on SiO_2 were used. At low electric laser fields, multiphoton ionization occurs, while at high electric fields, photon induced tunneling is obtained. (The curves in the respectively other region of electric laser field are only for illustration.) We choose a smooth transition for the strong-electric-field ionization rate $\dot{W}_{\mathrm{sefi}}$, represented by the solid line.

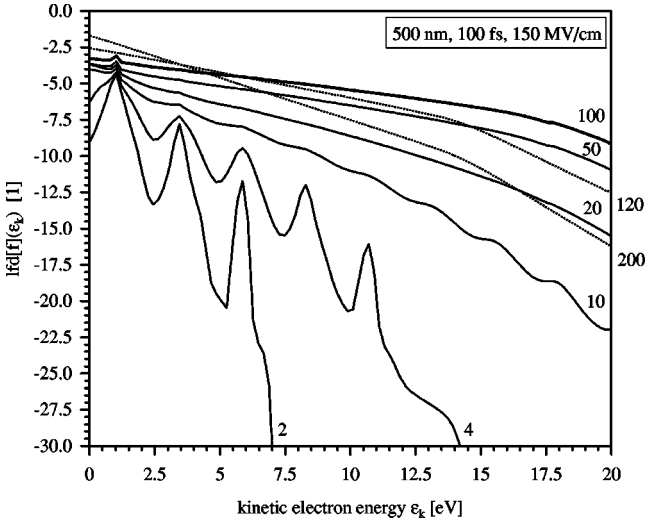

FIG. 3. Transient behavior of electron occupation number, represented by the function lfd[f] [see Eq. (22)]. Deviation from a straight line indicates disturbance of thermal equilibrium; the value of lfd[f](ε_k) represents the number of electrons in the corresponding energy state. The numbers at the curves are the time in femtoseconds from the beginning of laser pulse irradiation. For the calculation a laser beam with 100 fs pulse length and electric field of 150 MV/cm is applied on SiO_2.

rameter γ, which involves the ratio of laser frequency Ω and electric laser field E_L:

$$\gamma = \frac{\Omega \sqrt{m_{\mathrm{redu}} \Delta}}{e E_L}. \tag{12}$$

For comparably low electric fields and high laser frequencies ($\gamma \gg 1$), the case of multiphoton ionization is given, and the ionization rate can be approximated by[12]

$$\dot{W}_{\mathrm{multpt}} = \frac{2}{9\pi} \Omega \left(\frac{m_{\mathrm{redu}} \Omega}{\hbar} \right)^{3/2} \phi\left(\sqrt{2 l_{\mathrm{sefi}} - (2\tilde{\Delta}/\hbar\Omega)} \right) \times \exp\left\{ 2 l_{\mathrm{sefi}} \left(1 - \frac{1}{4\gamma^2} \right) \right\} \left(\frac{1}{16\gamma^2} \right)^{l_{\mathrm{sefi}}}, \tag{13}$$

where ϕ denotes Dawson's integral and $l_{\mathrm{sefi}} = \lfloor \tilde{\Delta}/\hbar\Omega + 1 \rfloor$ is the order of multiphoton ionization which is the largest integer below $\tilde{\Delta}/\hbar\Omega + 1$.

For high electric fields and low laser frequencies ($\gamma \ll 1$) the opposite case of photo-induced tunneling is represented. Keldysh obtained an approximation for the ionization rate as

$$\dot{W}_{\mathrm{pttunnel}} = \frac{2}{9\pi^2} \frac{\Delta}{\hbar} \left(\frac{m_{\mathrm{redu}} \Delta}{\hbar^2} \right)^{3/2} \left(\frac{\hbar\Omega}{\Delta\gamma} \right)^{5/2} \times \exp\left\{ -\frac{\pi}{2} \frac{\Delta\gamma}{\hbar\Omega} \left(1 - \frac{\gamma^2}{8} \right) \right\}. \tag{14}$$

In this work we consider a wide range of electric laser fields and thus both $\gamma \gg 1$ and $\gamma \ll 1$. For the transition between multiphoton ionization and photoinduced tunneling we apply a weighted linear combination of $\dot{W}_{\mathrm{multpt}}$ and $\dot{W}_{\mathrm{pttunnel}}$.

Figure 2 shows both ionization rates for multiphoton ionization (13) and photo-induced tunneling (14) as functions of the electric laser field for a laser with a wavelength of 500 nm and material parameters of SiO_2. Expression (13) is valid for laser fields below 50 MV/cm; Eq. (14) can be used for laser fields above approximately 200 MV/cm. Note that outside the regions of validity, unphysical results are obtained, for example the rate of photoinduced tunneling tends to infinity. The steps seen in the curve representing multiphoton ionization rate do have physical reasons and can be explained by the increase of ionization potential leading to a higher order of multiphoton ionization. We use a smooth transition $\dot{W}_{\mathrm{sefi}}$ between both approximations which is shown by the solid line in Fig. 2.

We use a separate collision term to include strong-electric-field ionization in our model. In contrast to rate equations considering only free-electron densities,[7,8,16,26] it is now possible to investigate explicitly the influence of this ionization process on the free-electron distribution function. In especial, the distribution of the shifted electrons by strong-electric-field ionization has a strong influence on the impact ionization because these seed electrons have initially a low kinetic energy (see Secs. V B and V D). Therefore they have to be heated above the critical energie ε_c [Eq. (7)] until they can perform impact ionization. When strong-electric-field ionization is implemented in rate equations or mean field equations instead, then these seed electrons are distributed over the whole energy spectrum which overestimates the amount of high-energy electrons.

Since photon momentum is much smaller than electron momentum, we can neglect a change of the electron's wave vector in this process. In the isotropic approximation with first order perturbation theory and assuming a filled valence band and a nearly empty conduction band, we obtain a linear relation between the ionization rate $\dot{W}_{\mathrm{sefi}}$ and the matrix element $|\mathcal{M}_{\mathrm{sefi}}(\varepsilon)|^2$ at energy ε:

$$|\mathcal{M}_{\text{sefi}}(\varepsilon)|^2=\frac{\pi\hbar^4\dot{W}_{\text{sefi}}}{\sqrt{2m^\star m_{\text{redu}}^2\varepsilon}}\delta_{\varepsilon_0,\varepsilon}. \tag{15}$$

Here $\varepsilon_0=(l_{\text{sefi}}\hbar\Omega-\tilde{\Delta})/(m^\star/m_v^\star+1)$ is the kinetic energy remaining for the free electron after overcoming the ionization potential. The collision integral then reads

$$\left(\frac{\partial f(\varepsilon)}{\partial t}\right)_{\text{sefi}}=\sqrt{2}\pi^2\left(\frac{\hbar}{\sqrt{m^\star}}\right)^3\dot{W}_{\text{sefi}}f_v(\varepsilon)(1-f(\varepsilon))\delta(\varepsilon_0-\varepsilon). \tag{16}$$

Because photon momentum is neglected, the collision integral is reduced to a δ distribution. This means that all electrons which are shifted into the conduction band by strong electric field ionization have the same amount of kinetic energy reflecting the δ distribution in their occupation number (see Sec. V B).

D. Electron-phonon collisions

Electron-phonon collisions are responsible for energy transfer from the excited electron gas to the phonon gas. Moreover, these collisions contribute for the disturbed electron gas to relax to thermal equilibrium. The interaction between the free electron gas and a nonpolar phonon gas is described with deformation potential theory, which is a valid approximation for long phonon wavelengths. This expression is, however, also applied to phonons with short wavelength. As a result, the free electrons interact only with longitudinal phonons. Because of diverse influence of electron scattering with acoustical or optical phonons due to the different phonon dispersion relations,[27] the acoustical and two optical phonon modes are taken into consideration and electron-phonon interactions are treated quantum mechanically.

For a collision in which a nonpolar longitudinal phonon of mode β with wave vector q is absorbed $(+)$ or emitted $(-)$, the matrix element reads[20,22,24]

$$\begin{aligned}|\mathcal{M}^{\pm}_{\text{e-ph-nonpol}}(\boldsymbol{k};(\boldsymbol{q},\beta);\boldsymbol{k}_1)|^2&:=|\langle\boldsymbol{k}_1|V^{\pm(\boldsymbol{q},\beta)}_{\text{e-ph}}|\boldsymbol{k}\rangle|^2\\&=\frac{\hbar}{2MN\omega_\beta(\boldsymbol{q})}\left(g_\beta(\boldsymbol{q})+\frac{1}{2}\mp\frac{1}{2}\right)|\boldsymbol{q}|^2C_D^2\delta_{\boldsymbol{k}_1,\boldsymbol{k}\pm\boldsymbol{q}},\end{aligned} \tag{17}$$

with momentum and energy conservation

$$\boldsymbol{k}_1=\boldsymbol{k}\pm\boldsymbol{q},\quad \varepsilon(\boldsymbol{k}_1)-\varepsilon(\boldsymbol{k})=\pm\hbar\omega_j(\boldsymbol{q}). \tag{18}$$

Here M is the mass of one of the N elementary cells of the crystal and $\omega_\beta(\boldsymbol{q})$ is the phonon's angular frequency. We use a deformation potential of $C_D=6$ eV for acoustical phonons as it was found from experimental results.[27] For optical phonons we apply the same matrix element, substituting C_D by the coupling constant $C_a=6$ eV.[27]

In ionic crystals a different matrix element, which can be deduced from Fröhlich Hamiltonian,[20,22,24] has to be used to describe the collision between free electrons and polar phonons.[32]

E. Absorption of laser energy by free electrons

Free electrons oscillate in the laser field and can absorb energy only when perturbed in this oscillation. The perturbation may occur, for example, when an oscillating electron collides with a phonon absorbing or emitting its momentum. Instead of using Joule heating of free electrons to treat laser absorption,[7,8,26] a quantum-mechanical approach is used because photon energy is comparable with the oscillation energy of a free electron in the electric laser field.[34] According to Epshtein[25] and Seely and Harris,[35] the matrix element of such a three-particle collision is given by

$$\begin{aligned}&|\mathcal{M}^{\pm}_{\text{e-ph-pt}}(\boldsymbol{k};(\boldsymbol{q},\beta);\boldsymbol{k}_1)|^2\\&\quad=|\mathcal{M}^{\pm}_{\text{e-ph}}(\boldsymbol{k};(\boldsymbol{q},\beta);\boldsymbol{k}_1)|^2\sum_{l=-\infty}^{\infty}J_l^2\left(\frac{e\boldsymbol{E}_L\cdot\boldsymbol{q}}{m^\star\Omega^2}\right)\\&\qquad\times\delta(\varepsilon(\boldsymbol{k}_1)-\varepsilon(\boldsymbol{k})\mp\hbar\omega_\beta(\boldsymbol{q})-l\hbar\Omega),\end{aligned} \tag{19}$$

where $\boldsymbol{E}_L$ is the vector of the electric laser field amplitude.

The index l stands for the number of photons being absorbed $(l>0)$ or emitted $(l<0)$ in one collision process. The probability of such a collision is given by the square of Bessel's function J_l. The term with $l=0$ provides the part of the pure electron-phonon interaction. If no laser field is applied $(\boldsymbol{E}_L=\boldsymbol{0})$ the matrix element reduces to the usual electron-phonon matrix element.

Using the assumption of a homogenous and isotropic crystal, and, since we do not consider a definite polarization of laser light, averaging over all directions of the electric laser field by defining $\overline{J_l^2}(q,E_0,\Omega):=\int_0^1J_l^2(eE_0q\mu/m^\star\Omega^2)d\mu$, the three-dimensional collision integral which represents light absorption by free electrons[18,25,32] can be reduced to one dimension, given by the following expression:[32]

$$\begin{aligned}\left(\frac{\partial f(\varepsilon)}{\partial t}\right)_{\text{e-ph-pt}}=&\frac{1}{4\pi\hbar^2}\frac{m^\star}{\varrho}\frac{1}{k(\varepsilon)}\sum_{\beta=0}^{b-1}\sum_{l=-\infty}^{\infty}\left\{\int_{\substack{q\leqslant q^\beta_{\max},q\in\mathcal{H}^\beta_+,\\ \varepsilon\geqslant-(l\hbar\Omega+\hbar\omega_\beta(q))\}}}dq\,\frac{C_\beta^2q^3}{\omega_\beta(q)}\overline{J_l^2}(q,E_0,\Omega)[f(\varepsilon_+)(1-f(\varepsilon))(s_\beta(q)+1)\right.\\&-f(\varepsilon)(1-f(\varepsilon_+))s_\beta(q)]+\int_{\substack{\{q\leqslant q^\beta_{\max},q\in\mathcal{H}^\beta_-,\\ \varepsilon\geqslant-(l\hbar\Omega-\hbar\omega_\beta(q))\}}}dq\,\frac{C_\beta^2q^3}{\omega_\beta(q)}\overline{J_l^2}(q,E_0,\Omega)\\&\left.\times[f(\varepsilon_-)(1-f(\varepsilon))s_\beta(q)-f(\varepsilon)(1-f(\varepsilon_-))(s_\beta(q)+1)]\right\},\end{aligned} \tag{20}$$

with $\varepsilon_{\pm}=\varepsilon\pm\hbar\omega_\beta(q)+l\hbar\Omega$ and $k(\varepsilon)=\sqrt{2m^\star\varepsilon/\hbar^2}$. Energy and momentum conservation result in boundary conditions which are described by the set $\mathcal{H}_{\pm}^{\beta}=[|k(\varepsilon)-k(\varepsilon_{\pm})|,k(\varepsilon)+k(\varepsilon_{\pm})]$. b is the number of the longitudinal phonon modes. ϱ is the density of material. Furthermore, there exists an upper limit for the phonon wave vector, thus the integration can only be carried out over q-values which are below $q_{\max}^{\beta}$. For acoustic phonons, $q_{\max}^{\beta}$ equals to Debye's phonon wave vector and C_β is the deformation potential, whereas for optical phonons these values have to be replaced by the wave vector of the Brillouin-zone boundary and the coupling constant, respectively.

In our calculations we apply electric laser field amplitudes of such magnitude that also Bessel functions of higher order may provide significant contributions. Since in the numerical calculations it is not possible to consider all terms of the sum, we have taken a pragmatic approach. By virtue of the identity $\Sigma_{l=-\infty}^{\infty}J_l^2=1$, we approximate the sum over negative l and the sum over positive l each by $[1/2(1-J_0^2)]$ and treat these expressions like photon emission and absorption of order one. In this way, we take higher order processes indirectly into account, however, underestimating the electron's energy gain. Nevertheless, the resulting energy gain using this approach is higher than if higher order processes $l\geqslant 3$ were completely neglected. Thus we replace $J_l^2(x)$ by $J_0^2(x)\,\delta_{0,l}+0.5(1-J_0^2(x))(\delta_{-1,l}+\delta_{1,l})$.

F. Boltzmann's equation for phonons

The Boltzmann equation for phonons contains only the collision term for phonon-electron-photon interaction, which can be calculated from the matrix element of electron-phonon-photon interaction (see Secs. III D and III E). Although phonons do not absorb energy from the laser, they are affected indirectly by irradiation due to their interaction with photon-absorbing electrons. This approach includes also pure phonon-electron interaction without laser irradiation. This three dimensional collision integral can also be reduced to one dimension and reads, in terms of phonon wave number q (Ref. 32)

$$\begin{aligned}\left(\frac{\partial g_\beta(q)}{\partial t}\right)_{\text{ph-e-pt}} &= \frac{1}{4\pi\hbar^4}\,\frac{(m^\star)^2}{\varrho}\,\frac{C_\beta^2 q}{\omega_\beta(q)}\\ &\times\sum_{\beta=0}^{b-1}\sum_{l=-\infty}^{\infty}\overline{J_l^2}(q,E_0,\Omega)\\ &\times\int_{\{\varepsilon\in\mathcal{G},\varepsilon\geqslant+l\hbar\Omega+\hbar\omega_\beta(q)\}}d\varepsilon\\ &\times[f(\varepsilon_+)(1-f(\varepsilon))(s_\beta(q)+1)\\ &-f(\varepsilon)(1-f(\varepsilon_+))s_\beta(q)],\end{aligned}\tag{21}$$

with $\varepsilon_+=\varepsilon+(l\hbar\Omega+\hbar\omega_\beta(q))$. The set $\mathcal{G}:=\{\varepsilon\geqslant 0:|q-k(\varepsilon_+)|\leqslant k(\varepsilon)\leqslant q+k(\varepsilon_+)\}$ constitutes boundary conditions due to momentum and energy conservation.

IV. SOLVING THE SYSTEM OF EQUATIONS

The system of nonlinear, coupled integro-differential equations [Eq. (2), Eq. (3) with the collision integrals from Sec. III] is solved numerically. We compute the electron occupation number f at 100 discrete energy values ε and the phonon occupation number g_β at 75 discrete phonon wave numbers q for each phonon mode β. Thus for SiO_2 we solve a system of 325 nonlinear, coupled ordinary differential equations numerically. For this we developed an algorithm in which the collision integrals are calculated for each time step. The step size is controlled automatically to ensure stable solutions. Thus we can observe the temporal evolution of the occupation numbers $f(\varepsilon)$ of electrons and $g_\beta(q)$ of phonons.

V. RESULTS FOR SiO_2

A. Parameters

All results shown in this article were calculated for a box-shaped laser pulse with wavelength $\lambda=500$ nm (photon energy $\hbar\Omega=2.48$ eV) shining on SiO_2 with bulklike material parameters. Pulse length and amplitude were varied.

B. Electron occupation number

Figure 3 shows the transient behavior of the occupation number of free electrons in the conduction band as a function of kinetic energy ε_k. The applied laser pulse has a length of 100 fs and an electric field of 150 MV/cm. The numbers at the curves denote the time in femtoseconds from the beginning of the pulse. The solid lines represent values of the occupation number during irradiation, whereas the dotted lines corresponds to values after the laser pulse.

Instead of f a function $\text{lfd}[f]$ is plotted, which is defined as

$$\text{lfd}[f](\varepsilon_k)=-\log\left(\frac{1}{f(\varepsilon_k)}-1\right).\tag{22}$$

In thermal equilibrium, when electrons obey a Fermi-Dirac distribution, $\text{lfd}[f](\varepsilon_k)$ equals $-(\varepsilon_k+\varepsilon_{\text{Fermi}}/2)/k_BT$. In this case $\text{lfd}[f](\varepsilon_k)$ is a linear function of electron energy ε_k with a slope proportional to the inverse electron temperature. Values of $\text{lfd}[f]$ increase monotonically with f values. The deviation of $\text{lfd}[f]$ from a straight line indicates the deviation of the electron gas from thermal equilibrium.

Immediately after the beginning of irradiation the occupation number in the conduction band starts to grow, as electrons are shifted from the valence band into the conduction band by strong-electric-field ionization, and thermal equilibrium is strongly disturbed.

Since the collision integral of strong-electric-field ionization is represented by a δ-function (Sec. III C) the shifted electrons have all the same kinetic energy reflected by a δ-peak in the occupation number at the bottom of the conduction band (low energies ε_k). As can be seen in Fig. 3, the $\text{lfd}[f]$-values for $t=4$ fs show a series of equally spaced peaks. The peak at the lowest energy results from electrons excited by strong-electric-field ionization. Some of these free electrons absorb further photons, resulting in an increased occupation number at energies larger by multiples of the photon energy. This leads to the formation of an equally spaced peak structure.

In the further course more and more electrons are promoted to the conduction band, where they continue absorb-

ing energy from laser irradiation. The peaklike structure, formed at the beginning of laser irradiation, is smeared out due to internal relaxation processes like electron-electron collisions. Also phonon heating by electron-phonon collisions leads to a relaxation of the electron gas. Already 50 fs after beginning of the laser pulse, no distinct peaks are visible except the lowest one caused by strong-electric-field ionization.

At the end of and after the laser pulse ($t \gtrsim 100$ fs) the high-energy part of the occupation number decreases while for low kinetic energies, the number of free electrons increases. This is an effect of impact ionization, where high-energy electrons partially transfer their energy to valence electrons. In such a collision, one high-energy electron disappears while two low-energy electrons emerge.

After irradiation, strong-electric-field ionization disappears whereas impact ionization still continues. Except for the high-energy tail the free-electron occupation number resembles an equilibrium distribution (linear lfd[f]-curve) by that time. The slope of the lfd[f]-curve decreases with time since the hot electron gas transfers energy to the lattice.

In contrast to results of Stuart *et al.*,[7,26] our calculations show that the free-electron occupation number distribution function changes its shape within the femtosecond regime.

C. Phonon occupation number

Figure 4 shows the transient behavior of the occupation number for each phonon mode. The same laser pulse as above is applied. The numbers at the curves represent the time in femtoseconds from the beginning of the pulse.

For each phonon mode the function lbe[g_β] is plotted as a function of the phonon wave vector. lbe[g_β] is defined as

$$\mathrm{lbe}[g_\beta](q) = -\log\left(\frac{1}{g_\beta(q)} + 1\right). \tag{23}$$

In thermal equilibrium when phonons obey a Bose-Einstein distribution, lbe[g_β](q) equals $-\hbar\omega_\beta(q)/k_B T$, thus (for Debye's model) lbe[g_β](q) is a linear function of the phonon wave vector q. For the acoustic mode, the slope is inversely proportional to the phonon temperature, whereas for optical modes the lbf[g_β]-curve represents a constant which is also proportional to the inverse phonon temperature. lbe[g_β] is an increasing, monotonic function of g_β.

As can be seen in Fig. 4 phonons of each mode are excited during ($t=0$ fs to 100 fs) and after laser pulse ($t=200$ fs) as the phonon gas gains energy from electron gas by electron-phonon collisions. In this process, phonons are created thus the occupation numbers grow across the whole wave vector spectrum. The smaller excitation at low wave vectors is an artifact of deformation potential theory. The disturbance from thermal equilibrium can be considered as small.

D. Ionization processes

Figure 5 shows the time dependence of the free-electron density during and after the laser pulse, and the contributions of strong-electric-field ionization and impact ionization, respectively. Four different pulse lengths have been treated, all

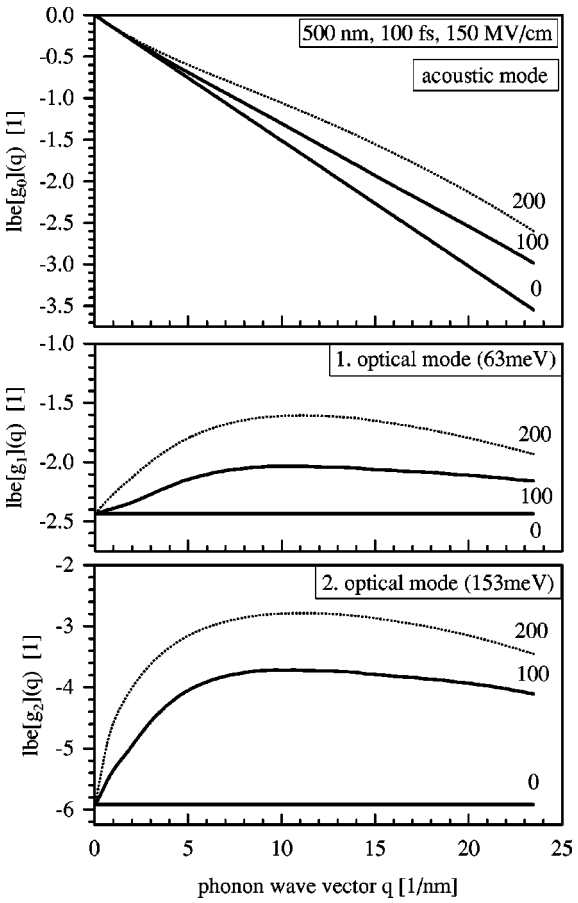

FIG. 4. Transient behavior of the phonon occupation number of the acoustic and the two optical modes, represented by the function lbe[g_β] [see Eq. (23)]. Its deviation from a straight line indicates disturbance of thermal equilibrium; the value of lbe[g_β](q) represents for each mode β the number of phonons in the corresponding wave vector state. The numbers at the curves are the time in femtoseconds from the beginning of laser pulse irradiation. For the calculation a laser beam with 100 fs pulse length and an electric field of 150 MV/cm is applied on SiO_2.

at an electric laser field of 150 MV/cm. Note the different scales on both axes of the figures.

The rate for strong-electric-field ionization is directly connected with the laser field [Eqs. (13) and (14)]. Since a box-shaped pulse is applied, this ionization rate increases linearly as a function of time until the laser pulse is over.

In contrast, impact ionization becomes important only when a sufficient number of high-energy electrons is present in the conduction band. Therefore this process starts much later than strong-electric-field ionization. Because each striking electron shifts a second electron into the conduction band, the density contribution of impact electrons grows exponentially.

However, for very short pulses of 25 fs, free electrons have not enough time during the irradiation to continue absorbing laser energy until they are heated above the critical energy for impact ionization [Eq. (7)]. In this case, the contribution of impact ionization to the electron density is negligible. If the laser pulse length is increased, the number of free electrons created by impact ionization also increases. Only for pulse lengths of 200 fs (and more) is the contribu-

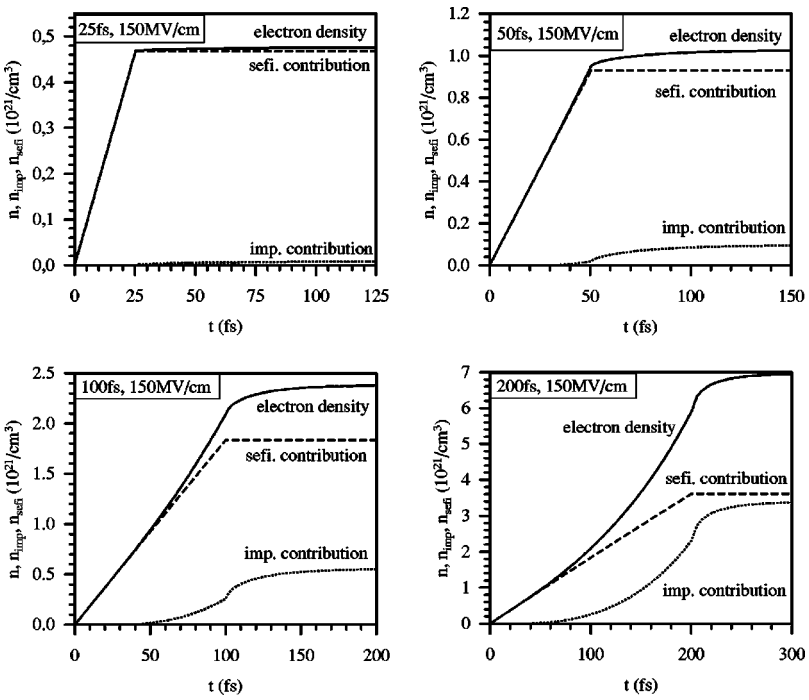

FIG. 5. Time dependence of free-electron density and the contributing processes, i.e., strong-electric-field ionization and impact ionization. A 500 nm laser pulse impinging on SiO_2 with an electric field of 150 MV/cm and pulse lengths of 25 fs, 50 fs, 100 fs, and 200 fs, respectively, are assumed.

tion of impact electrons comparable to (in excess of) the contribution of the strong electric field ionization.

The figures show a sharp rise in impact ionization at the end of laser irradiation. This is caused by the sharp decrease of the ionization potential $\tilde{\Delta}$, Eq. (1). When the electric laser field is switched off, the critical energy ε_c [Eq. (7)] drops to a lower value. (Obviously, this is an artifact of our box-shaped pulse.)

Impact ionization continues for about $\sim$ 100 fs after irradiation. Eventually, no electrons remain in the conduction band with sufficient energy for impact ionization, and the electron density saturates. (In reality it would decrease due to recombination which, however, is not included in our model.)

Although in Sec. III B we concluded that our matrix element for impact ionization should yield stronger impact ionization in comparison to other authors,[7,26] our approach with collision integrals leads to unexpected low impact ionization rates. We assume that Keldysh's formula cannot be used for the studied case, because our results show that a huge part of impact ionizated electrons are produced by free electrons with kinetic energies much larger than critical energy ε_c [Eq. (7)]. An additional effect reducing the possibility of impact ionization is the consideration of energy conservation and momentum conservation in our approach. Therefore, we do not obtain an avalanche of impact ionization. Nevertheless, as will be shown below, we obtain free electron densities which are high enough for dielectric breakdown and damage thresholds in good agreement with experimental results.

We varied the applied parameters by increasing effective electron mass in valence band $m_v^\star$ or decreasing band gap Δ. Both leads to an increase of impact ionization. However, strong-electric-field ionization still remains the dominant ionization process for laser pulses below 150 fs.

For example, when $m_v^\star$ is doubled, then, for a laser pulse of 100 fs duration at 150 MV/cm, the contribution to free-electron density through impact ionization increases about 21%, whereas the contribution by strong-electric-field ionization decreases about 22% and the ratio of impact ionization to strong-electric-field ionization raises from 0.3 to 0.47.

For the same laser pulse, a reduction of the band gap from 9 eV to 6 eV leads to an increase of both ionization processes. The numbers of ionized electrons raises by factor 6.3 for impact ionization, and by a factor 2.5 for strong-electric-field ionization. The total free-electron density increases by a factor of about 3.35 and the above ratio of impact ionization to strong-electric-field ionization is then 0.77.

Thus, the width of band gap strongly influences the strengths of both ionization processes and therefore plays a significant role in determining damage threshold using density criterion.

Figure 6 shows the time derivative of the contribution of impact ionization of free-electron density $\partial n_{\mathrm{imp}}/\partial t$ as a function of free-electron density n for different pulse lengths in the femtosecond regime.

The same pulse parameters as in Fig. 5 were applied. For all assumed pulse lengths, the impact ionization rate increases during irradiation with increasing free-electron density. The time period of the pulse is represented by the smooth increase of impact ionization rate. The sharp rise in the ionization rate, as described above, marks the end of irradiation. Also the final saturation of impact ionization at slightly higher electron densities than those which are obtained during the pulse can be observed.

For pulse lengths in the range of picoseconds, it is commonly assumed that impact ionization grows exponentially and can be described by

$$\partial n_{\mathrm{imp}}/\partial t = \alpha(E_L) n, \tag{24}$$

where α is the so-called avalanche coefficient.[11,16,36] Thus, for a box-shaped laser pulse as applied in our work, a linear increase of impact ionization rate with free-electron density is expected during the pulse. As Fig. 6 shows, the simple rate equation (24) does not hold for pulse durations in the fem-

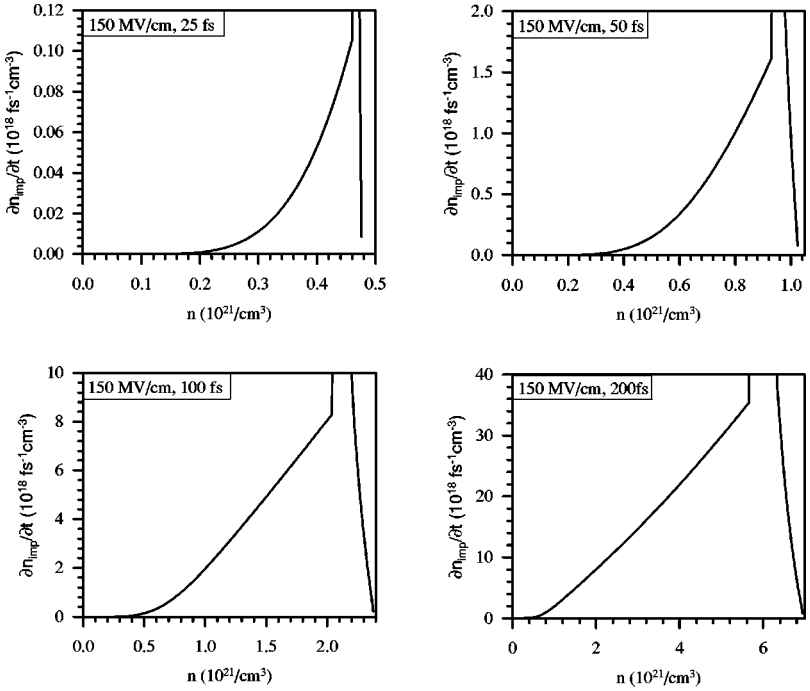

FIG. 6. Time derivative of the contribution of impact ionization of free-electron density as a function of the free-electron density for different pulse lengths, 25 fs, 50 fs, 100 fs, and 200 fs, respectively. A 500 nm laser pulse impinging on SiO_2 with an electric field of 150 MV/cm is assumed.

tosecond regime. The description of $\partial n_{\mathrm{imp}}/\partial t$ proportional to n is justified only for free-electron densities higher than $n \sim 6\times10^{20}$ cm^{-3} and therefore not applicable to calculate the initial evolution of the free-electron density. The linear regime is not reached when assuming a pulse of 25 fs duration. For the 100 fs pulse, linearity is reached after about half of total pulse duration. Only for pulse lengths of 200 fs (and more), a linear dependence of impact ionization rate on free-electron density, according to Eq. (24), can be assumed for the whole pulse duration. This result only slightly depends on the applied electric laser field.

Thus, the energy dependence of impact ionization and the time needed for free-electron heating up to critical energy (7) play a significant role in femtosecond laser irradiation of dielectrics. We obtain a stronger restriction of the applicability of Eq. (24) than other authors,[11,26,36] because we included momentum conservation and a effective ionization potential, obtaining a higher critical energy (7).

Figure 7 shows the maximum free-electron density in SiO_2 depending on the electric laser field. The individual contributions to the free electron density from strong-electric-field ionization and impact ionization, respectively, are also plotted.

For all investigated pulse lengths, the electron density increases with increasing electric laser field: Strong-electric-field ionization is directly proportional to the laser pulse intensity [Eqs. (13) and (14)], whereas the impact ionization rate increases because of the avalanche effect.

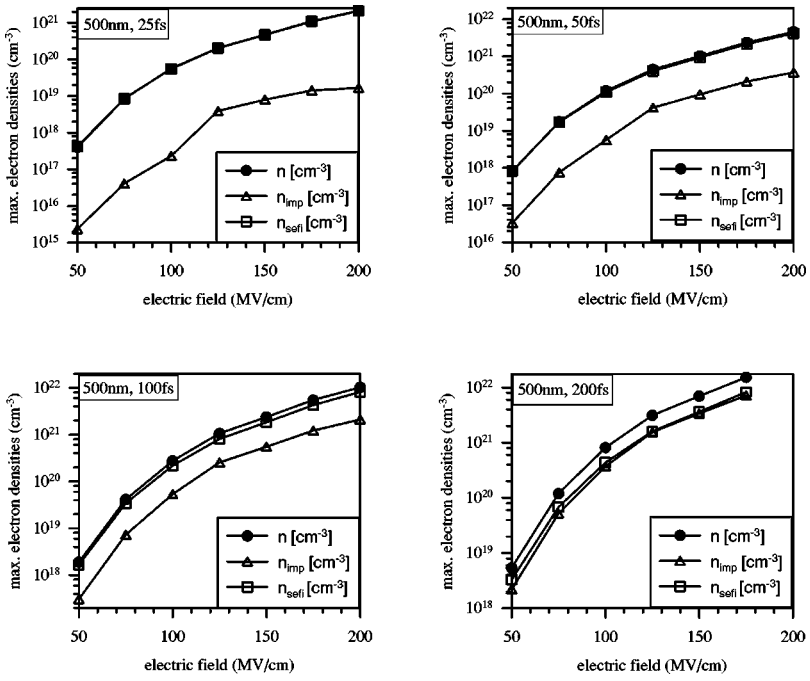

FIG. 7. Maximum electron density in the conduction band after laser irradiation for varying electric laser fields, together with contributions from the two considered ionization processes. The four figures represent four different laser pulse durations.

The figure shows that for pulse lengths below ~100 fs the contribution of impact ionization is negligible compared to strong-electric-field ionization. Only for a pulse length of 200 fs do both processes provide similar contributions. Thus the pulse length determines predominantly which ionization process is mainly responsible for the formation of a free electron gas.

A commonly used criterion of an ablation threshold is plasma formation, where the dielectric is assumed to change to plasma state when the electron density exceeds a critical value.[1,5,7]

The calculations underlying Fig. 7 were continued up to the critical plasma density $n_P=\epsilon_r\epsilon_0 m^\star\Omega^2/e^2$, at which the real part $\mathrm{Re}\,\epsilon(\Omega)$ of the dielectric function $\epsilon(\Omega)$ becomes zero, i.e., the laser beam gets totally reflected. Here ϵ_r is the specific dielectric constant, n_P is determined by $\mathrm{Re}\,\epsilon(\Omega)=\epsilon_r-(\omega_P/\Omega)^2=0$ with $\omega_P=(ne^2/(\epsilon_0 m^\star))^{1/2}$.[37]

Note that our model is only valid for free electron densities at which electron-ion collisions are negligible. If the free electron density reaches a certain value, which is below the critical plasma density, the collisions of free electron with ions (inverse bremsstrahlung) have to be included because then this process occurs with higher probability than electron-phonon collisions.[38] Then absorption will increase even more with increasing electron density.

To determine the damage threshold fluence $F=I_{\mathrm{vac}}\tau$, first, the vacuum intensity needs to be calculated from the electric field E_L within the material. The intensity I_{bulk} within the bulk reads $I_{\mathrm{bulk}}=\sqrt{\epsilon_0/\mu_0}\sqrt{\mathrm{Re}\,\epsilon(\Omega)}E_L^2$.[39] In case of small absorption, $\mathrm{Re}\,\epsilon(\Omega)$ is given by the refraction index n_r, $\sqrt{\mathrm{Re}\,\epsilon(\Omega)}\approx n_r$. The vacuum intensity I_{vac} can be calculated by $I_{\mathrm{vac}}=(1-R)I_{\mathrm{bulk}}$ using the reflection coefficient $R=|(\hat{n}_r-1)/(\hat{n}_r+1)|^2$, where $\hat{n}_r=n_r-ik$ is the complex refraction index. Well below the specific plasma density, as mentioned above, the absorption coefficient is small compared to the refraction index, $\hat{n}_r\approx n_r$, and I_{vac} reads

$$I_{\mathrm{vac}}=\left(\frac{n_r+1}{2}\right)^2\sqrt{\frac{\epsilon_0}{\mu_0}}E_L^2. \tag{25}$$

In experiments the intensity I_{vac} is the known parameter. Equation (25) is valid in prebreakdown regime, when the electron density is up to one third of the critical plasma density. For this electron density the electric field increases with increasing electron density and constant intensity I_{vac}. Increasing the electric field, in turn, leads to an increasing electron density, so that the breakdown regime is quickly reached.

We use a free electron density of $n_c=10^{21}\ \mathrm{cm}^{-3}$, as damage criterion,[5,7] which is somewhat below the critical plasma density, hence Eq. (25) is still applicable. The precise choice of n_c has only a weak influence on the calculated damage threshold. For a box-shaped pulse and a critical density n_c, we obtain with $n_r=1.55$[40] for photon energy of 2.5 eV, $\mu_r=1$ the damage thresholds shown in Fig. 8.

These calculated damage thresholds are of the same magnitude and show the same qualitative dependence on laser pulse duration as experimental results.[5–7,11]

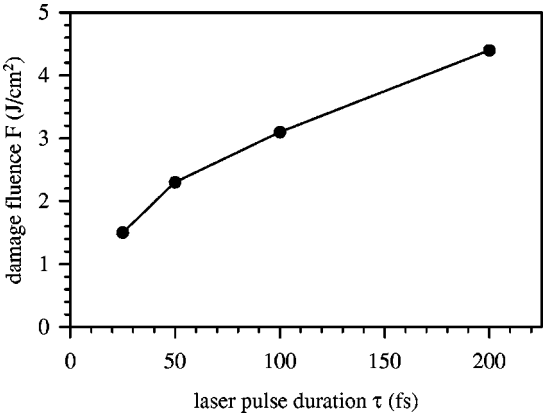

FIG. 8. Calculated damage threshold for a laser pulse with wavelength of 500 nm irradiating SiO_2. A free electron density of 10^{21} 1/cm^3 is used as damage criterion.

E. Internal energy

For a laser pulse with a duration of 100 fs and an electric field of 150 MV/cm we show in Fig. 9 the transient behavior of the total deposited energy together with the internal energy increase of the free electron gas and the internal energy of the phonon gas. The internal energy of the electron gas is calculated by integration over the *kinetic* energy of free electrons. However, the *total* energy absorbed by electrons is higher by the part of laser energy used to overcome the ionization potential. We approximate the total energy deposited in the crystal by adding the product of the free electron density with the bandgap to the sum of the internal electron energy and the phonon energy.

The total energy deposited in the crystal increases immediately when irradiation starts. This initial contribution is solely due to strong-electric-field ionization providing free electrons of low kinetic energy. The internal kinetic energy of electrons grows later due to phonon assisted photon absorption by free electrons. Therefore, the initially linear growth of total energy becomes progressive in the further course. Ionization processes continue to generate free electrons, which in turn continue to absorb photons, thereby increasing their kinetic energy. The internal energy of the phonon gas rises later and more moderately, because the only considered process of phonon heating is through direct

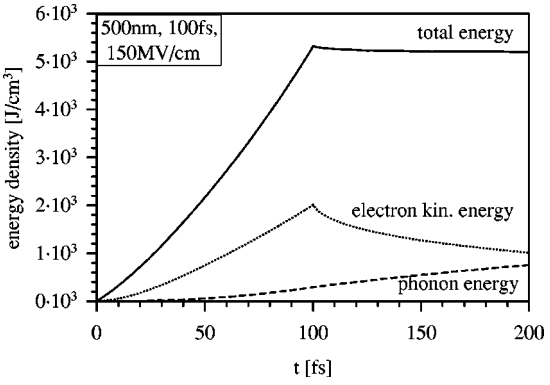

FIG. 9. Time dependence of internal energy of the free-electron gas (dotted line), phonon gas (dashed line), and total absorbed laser energy (solid line). The calculation is performed for a laser pulse with electric field of 150 MV/cm and pulse length of 100 fs.

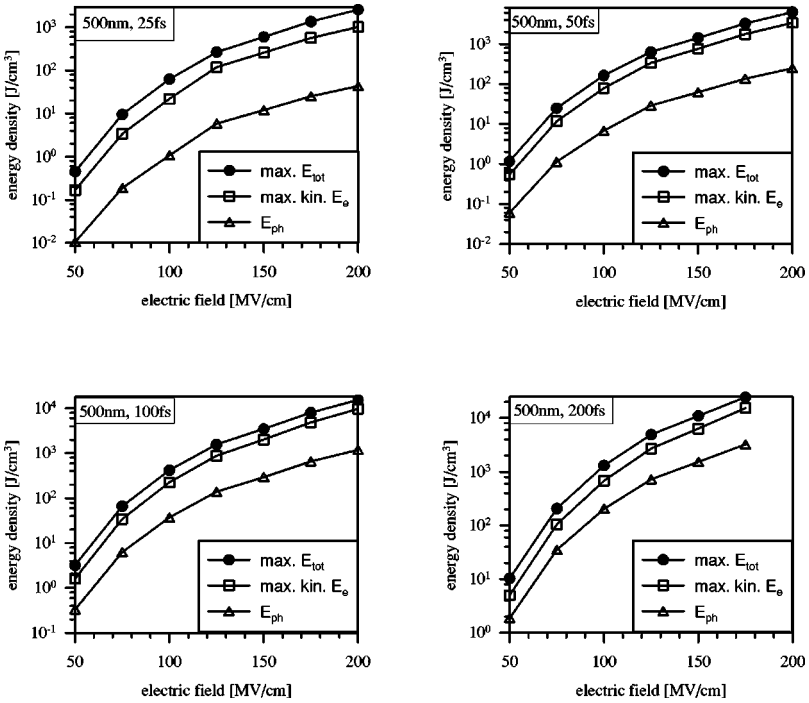

FIG. 10. Electric laser field dependence of total absorbed energy, internal energy of free electron gas and of phonon gas, respectively, at the end of the pulse. Four different pulse lengths were assumed.

electron-phonon collisions, which are rather inefficient with regard to energy transfer. The contributions of acoustical and optical phonon modes are nearly equal.[32]

After irradiation, the total deposited energy remains constant. The slight decrease seen in the figure is a numerical artifact. In fact, conservation of the total energy is a useful check of numerical stability. The kinetic energy of the electron gas decreases through two processes. First, in impact ionization, kinetic energy is used to overcome the bandgap. Second, energy is transferred from the electron gas to the phonon gas. This process continues long time after irradiation until the electron temperature equals phonon temperature. (Since our model does not include recombination we have the same situation as described by the two-temperature model for metals.[41] Note that equality of temperatures does not imply equality of internal energies due to the large difference of heat capacities.)

When comparing the excited, nonequilibrium electron gas with an electron gas with the same internal energy content at equilibrium, we find that the corresponding equivalent electron temperature reaches up to 40 000 K. However, note when the free electron gas is not in equilibrium, this quantity has no direct physical meaning of temperature. The temperature increase of the phonon gas, on the other hand, is found to be only a few 100 K. We can estimate the maximum temperature increase of the lattice at the end of the pulse, by assuming that *all* energy deposited into the crystal will be contained in the lattice, for example, via nonradiating recombination processes. In this way we obtain a maximum temperature increase of 2500 K of the SiO_2 lattice, which is above breakup temperature [crystalline quartz decays at atmospheric pressure at a temperature of 1997 K (Ref. 28)]. Note that this is an upper limit not only because of the above assumptions, but also because we do not account for heat conduction in our model.

The final total energy deposited in the crystal, the maximum value of internal kinetic energy of the free-electron gas and the phonon energy at the end of laser irradiation, are shown in Fig. 10 as functions of the electric laser field. The calculations were performed for the four different pulse lengths as in Fig. 7.

All investigated types of energy amount increase with electric laser field and duration of irradiation. The internal energy of the phonon gas at the end of the pulse is always much smaller than the internal energy of electron gas, which in turn differs from the total amount of deposited energy. The heating of the phonon gas at the end of the pulse is rather small for most investigated parameters, thus the internal energy is not sufficient for melting or even evaporation during the pulse. (For SiO_2, the lattice temperature in Kelvin can be estimated by half of the value of the energy density in J/cm^3.) Using the above approximation to calculate the upper limit of temperature increase, we find that for pulses with $\tau_L \gtrsim 50$ fs, lattice temperatures far above breakup temperature may be reached.

The estimated fluences necessary to reach breakup temperature show the same qualitative dependence on pulse duration as the threshold fluences to reach critical electron density (see Sec. V D). The values are higher than those of Sec. V D, although of the same order of magnitude. Keep in mind that the fluence to reach breakup temperature is only a rough estimate because we considered only intrinsic mechanisms for laser absorption of a perfect (unreal) crystal. Moreover, to investigate lattice damage in particular, processes like bond breaking due to high electron density[42–44] and intrinsic effects like defect creation by recombination[2,3,9] have to be considered.

VI. CONCLUSION

We investigated irradiation of dielectrics with subpicosecond laser pulses using a kinetic description. Thus, effects of particular collision processes on macroscopic material response can be studied even for a highly nonequilibrium elec-

tron gas. An appropriate system of coupled, time-dependent Boltzmann equations is solved numerically. Collision terms for strong-electric-field ionization and impact ionization are included. Our model enables us to investigate intrinsic absorption processes as basic mechanisms for dielectric breakdown. In contrast to other kinetic approaches,[7,8,15,18,19,26] we explicitly calculate the transient free electron distribution and phonon distribution by microscopic collision integrals avoiding any phenomenological or averaging parameter.

The results for SiO_2 irradiated by a single laser pulse of femtosecond duration demonstrate the high-nonequilibrium state of the electron gas and phonon gas during and after laser irradiation. The free-electron gas is formed mainly by strong-electric-field ionization, whereas impact ionization is of minor importance for laser pulses below 100 fs. Only at pulses about 200 fs does the contribution to free electron density by impact ionization become as important as strong-electric-field ionization. In contrast to other approaches,[7,16] our description of ionization processes includes momentum conservation and an appropriate effective ionization potential resulting in a higher critical energy for impact ionization, therefore we do not obtain an electron avalanche. Impact ionization is restricted to a small period at the end of and after the pulse because only then are energetic free electrons available. Thus, a duration of irradiation of 200 fs and lower appears too short for an electron avalanche to develop. Simple rate equations used by many authors to estimate the free electron density disregard the energy dependence of impact ionization. We have shown that such equations are not applicable to femtosecond laser irradiation, therefore they can lead to wrong results.

We have estimated threshold fluences using several criteria for damage threshold as critical electron density and total absorbed energy. The resulting damage thresholds are in good agreement with experimental measurements.[5–7,11]

ACKNOWLEDGMENTS

The authors would like to thank S. I. Anisimov, Landau Institute Moscow, Russia, D. Ashkenasi, Max-Born Institute Berlin, Germany, A. M. Rubenchik, Lawrence Livermore National Laboratory, CA, and K. Sokolowski-Tinten, University of Essen, Germany for their stimulating discussions.

*Electronic address: kaiser@mpipks-dresden.mpg.de
†Electronic address: brf@ilp.physik.uni-essen.de

[1] N. Bloembergen, IEEE J. Quantum Electron. **QE-10**, 375 (1974).
[2] A.A. Manenkov and A.M. Prokhorov, Usp. Fiz. Nauk **29**, 179 (1986) [Sov. Phys. Usp. **29**, 104 (1986)].
[3] S.C. Jones, P. Bräunlich, R.T. Casper, X.-A. Sheen, and P. Kelly, Opt. Eng. **28**, 1039 (1989).
[4] C. Quoix, G. Grillon, A. Antonetti, J.-P. Geindre, P. Audebert, and J.-C. Gauthier, Eur. Phys. J.: Appl. Phys. **5**, 163 (1999).
[5] D. von der Linde and H. Schüler, J. Opt. Soc. Am. B **13**, 216 (1996).
[6] H. Varel, D. Ashkenasi, A. Rosenfeld, R. Herrmann, F. Noack, and E.E.B. Campbell, Appl. Phys. A: Mater. Sci. Process. **62**, 293 (1996).
[7] B.C. Stuart, M.D. Feit, S. Herman, A.M. Rubenchik, B.W. Shore, and M.D. Perry, Phys. Rev. B **53**, 1749 (1996).
[8] B.C. Stuart, M.D. Feit, S. Herman, A.M. Rubenchik, B.W. Shore, and M.D. Perry, J. Opt. Soc. Am. B **13**, 459 (1996).
[9] G. Petite, P. Daguzan, S. Guizard, and P. Martin, Nucl. Instrum. Methods Phys. Res. B **107**, 97 (1996).
[10] S. Anisimov and V. Khokhlov, *Instabilities in Laser Matter Interaction* (CRC Press, Boca Raton, 1995).
[11] M. Lenzner, J. Krüger, S. Sartania, Z. Cheng, Ch. Spielmann, G. Mourou, W. Kautek, and F. Krausz, Phys. Rev. Lett. **80**, 4076 (1998).
[12] L.V. Keldysh, Zh. Éksp. Teor. Fiz. **47**, 1945 (1964) [Sov. Phys. JETP **20**, 1307 (1965)].
[13] A.V. Vinogradov and F.S. Faizullov, Sov. J. Quantum Electron. **7**, 650 (1977).
[14] A.S. Epifanov, Zh. Éksp. Teor. Fiz. **67**, 1805 (1974) [Sov. Phys. JETP **40**, 897 (1975)].
[15] B.G. Gorshkov, A.S. Epifanov, and A.A. Manenkov, Zh. Éksp. Teor. Fiz. **76**, 617 (1979) [Sov. Phys. JETP **49**, 309 (1979)].
[16] D. Arnold and E. Cartier, Phys. Rev. B **46**, 15 102 (1992).
[17] L.V. Keldysh, Zh. Éksp. Teor. Fiz. **11**, 509 (1960) [Sov. Phys. JETP **11**, 369 (1960)].
[18] A.S. Epifanov, A.A. Manenkov, and A.M. Prokhorov, Zh. Éksp. Teor. Fiz. **70**, 728 (1976) [Sov. Phys. JETP **43**, 377 (1976)].
[19] M. Sparks, D.L. Mills, R. Warren, T. Holstein, A.A. Maradudin, L.J. Sham, E. Loh, Jr., and D. F. King, Phys. Rev. B **24**, 3519 (1981).
[20] M.V. Fischetti, D.J. DiMaria, S.D. Brorson, T.N. Theis, and J.R. Kirtley, Phys. Rev. B **31**, 8124 (1985).
[21] E. Cartier and F.R. McFeely, Phys. Rev. B **44**, 10 689 (1991).
[22] A. Haug, *Theoretische Festkörperphysik I, II* (Fr. Deuticke, Wien, 1970).
[23] B. Ridley, *Quantum Processes in Semiconductors* (Clarendon, Oxford, 1993).
[24] J.M. Ziman, *Electrons and Phonons–The Theory of Transport Phenomena in Solids*, 2nd ed. (Clarendon, Oxford, 1962).
[25] E.M. Epshtein, Fiz. Tverd. Tela (Leningrad) **11**, 1787 (1970) [Sov. Phys. Solid State **11**, 2213 (1970)].
[26] B.C. Stuart, M.D. Feit, A.M. Rubenchik, B.W. Shore, and M.D. Perry, Phys. Rev. Lett. **74**, 2248 (1995).
[27] D. Arnold, E. Cartier, and D.J. DiMaria, Phys. Rev. B **49**, 10 278 (1994).
[28] I.S. Grigorev and E.Z. Mejlikhov, *Fizicheskie Velichini* (Energoatomizdat, Moscow, 1991).
[29] M.V. Fischetti, Phys. Rev. Lett. **53**, 1755 (1984).
[30] R. Binder, H.S. Köhler, M. Bonitz, and N. Kwong, Phys. Rev. B **55**, 5110 (1997).
[31] C.-K. Sun, F. Vallée, L.H. Acioli, E.P. Ippen, and J.G. Fujimoto, Phys. Rev. B **50**, 15 337 (1994).
[32] A. Kaiser, Diplom thesis, Technische Universität Braunschweig, 1998.
[33] D.W. Snoke, W.W. Rühle, Y.-C. Lu, and E. Bauser, Phys. Rev. B **45**, 10 979 (1992).
[34] Y.B. Zel'dovich and Y.P. Raĭzer, Zh. Éksp. Teor. Fiz. **47**, 1150 (1964) [Sov. Phys. JETP **20**, 772 (1965)].
[35] J.F. Seely and E.G. Harris, Phys. Rev. A **7**, 1064 (1973).
[36] A.-C. Tien, S. Backus, H. Kapteyn, M. Murnane, and G. Mourou, Phys. Rev. Lett. **82**, 3883 (1999).
[37] K. Sokolowski-Tinten, J. Bialkowski, M. Boing, A. Cavalleri, and D. von der Linde, Phys. Rev. B **58**, R11 805 (1998).

[38] B. Rethfeld, Ph.D. thesis, Technische Universität Braunschweig, 1999.
[39] L.D. Landau and E.M. Lifschitz, *Course of Theoretical Physics Vol. 8: Electrodynamics of Continuous Media* (Pergamon, Oxford, 1960).
[40] E.D. Palik, *Handbook of Optical Constants of Solids* (Academic, New York, 1985).
[41] S.I. Anisimov, B.L. Kapeliovich, and T.L. Perelman, Zh. Éksp. Teor. Fiz. **66**, 776 (1974) [Sov. Phys. JETP **39**, 375 (1974)].
[42] P. Stampfli and K.H. Bennemann, Phys. Rev. B **46**, 10 686 (1992).
[43] P. Stampfli and K.H. Bennemann, Phys. Rev. B **49**, 7299 (1994).
[44] P.L. Silvestrelli, A. Alavi, M. Parrinello, and D. Frenkel, Phys. Rev. Lett. **77**, 3149 (1996).